Particle transport behavior in air channel flow with multi-group Lagrangian tracking*

Hao Lu(卢浩)[1], Wen-Jun Zhao(赵文君)[2,†], Hui-Qiang Zhang(张会强)[1], Bing Wang(王兵)[1], and Xi-Lin Wang(王希麟)[1]

[1] School of Aerospace Engineering, Tsinghua University, Beijing 100084, China
[2] Faculty of Architecture, The University of Hong Kong, Hong Kong, China

(Received 30 June 2016; revised manuscript received 18 August 2016; published online 29 November 2016)

The particle motions of dispersion and transport in air channel flow are investigated using a large eddy simulation (LES) and Lagrangian trajectory method. The mean and fluctuating velocities of the fluids and particles are obtained, and the results are in good agreement with the data in the literature. Particle clustering is observed in the near-wall and low-speed regions. To reveal the evolution process and mechanism of particle dispersion and transport in the turbulent boundary layer, a multi-group Lagrangian tracking is applied when the two-phase flow has become fully developed: the fluid fields are classified into four sub-regions based on the flow characteristics, and particles in the turbulent region are divided accordingly into four groups when the gas–particle flow is fully developed. The spatiotemporal transport of the four groups of particles is then tracked and analyzed. The detailed relationship between particle dispersion and turbulent motion is investigated and discussed.

Keywords: particle-laden flows, channel flow, large-eddy simulations, coherent structures

PACS: 47.55.Kf, 47.27.nd, 47.27.ep, 47.27.De **DOI:** 10.1088/1674-1056/26/1/014702

1. Introduction

Particle-laden air channel flow is an important issue in many natural and industrial processes, such as pneumatic conveying systems, fluidized beds, pollutant particle transport in atmospheric boundary layers, and fuel particle dispersion in combustors.[1–3] It is also the foundation of gas–particle two-phase turbulent combustion in many industrial processes.[4,5] Therefore, it is vital to understand the processes and mechanisms of particle dispersion and transport in turbulent airflows to apply industry controls and improve combustion efficiency.

The influence of fluid motion on aerosol particle behavior is crucial in predicting particle dispersion and transport.[5] Traditional theories assume that particles are randomly distributed in turbulent flows according to the diffusion of passive scalars. However, Crowe *et al.*, Squires and Eaton, and Wang and Maxey have found that there are highly nonuniform concentration distributions of particles in turbulent flow fields.[6–11] This inhomogeneous spatial distribution of particles in turbulent flow, known as preferential concentration,[8,9] is caused by differences in inertia between particles and fluids. Moreover, turbulent motion and particle properties are two key factors determining the preferential concentration of particles.[12–18]

The particle distribution and transport are mainly controlled by turbulent motion and structures. McLaughlin[19] and Brooke *et al.*[20] found that particles tend to accumulate in the viscous sublayer near the wall. Eaton and Fessler[21] identified the mechanism driving preferential concentration as the centrifuging of particles away from turbulent vortex cores. Kaftori *et al.*[22,23] investigated the motion of solid particles near the wall in a turbulent boundary layer using flow visualization techniques. They found that particles are controlled by the actions of coherent wall structures. Tanaka *et al.* [24] found that the interaction between particle clusters and vortical structures plays an essential role in the nonuniform distribution of particles when the particle response time is of the order of the Kolmogorov timescale.

In addition, the Stokes number of the aerosol particles, St, also plays an important role in how the particles respond to turbulent motion. St is defined as the ratio of particle relaxation time to the Kolmogorov timescale of turbulent flow ($St = \tau_{\mathrm{rp}}/\tau_{\mathrm{f}}$). Wang and Maxey[10,11] showed that the strongest accumulation of particles occurs when the particle response time is comparable to the Kolmogorov timescale. Fessler *et al.*[25] imaged the distributions of particles in turbulent flow and found the strongest preferential concentration for $St = 1$. Wang and Squires[26] investigated particle transport in fully developed turbulent flow using a numerical simulation. They found that particles for $St = 1$ exhibit preferential concentration near the wall and appear more nonuniform than particles with other St values.

In summary, it has been confirmed that particles accumulate in the specific regions of turbulent flow fields and that the

*Project supported by the Key Program of the National Natural Science Foundation of China (Grant No. 11132005) and the National Natural Science Foundation of China (Grant No. 50876053).

†Corresponding author. E-mail: zhaowenjunhku@gmail.com

© 2017 Chinese Physical Society and IOP Publishing Ltd

strongest preferential concentration occurs for particles with $St = 1$. However, the detailed particle dispersion behavior and transport mechanism in turbulent flow are not well understood and require further investigation.[27] In the present study, the particle dispersion and transport is examined in a three-dimensional fully developed turbulent airflow by means of a large eddy simulation (LES) coupled with the Lagrangian trajectory method. The objective of this study is to understand how particles are transported into the specific accumulation regions of turbulent flow fields and why they can maintain a high concentration in these regions. A better understanding of these issues will be useful and important for further industrial design and engineering applications. As it has been found that particles with $St = 1$ present strongly nonuniform concentration distributions in turbulent flow,[25,26] we focus on analyzing and discussing this specific case.

To reveal the spatiotemporal transport process and mechanism of particles in turbulent flow, a multi-group Lagrangian method is proposed: at some specified time, the fully developed airflow fields are split into four sub-regions according to the flow characteristics. The particles are divided into four groups based on their positions in the flow fields. The trajectories of the multi-groups of particles in the different flow sub-regions are then tracked. The detailed evolution processes involved in particle dispersion and clustering toward the wall are analyzed and discussed, and then the mechanisms of particle accumulations in the specific flow regions are investigated over long time periods.

2. Numerical methods

2.1. Large eddy simulation of the airflow fields

A particle-laden turbulent airflow is simulated in a symmetric channel, as shown in Fig. 1. The channel dimensions are $2\pi h$, $2h$, and πh in the streamwise (x), wall normal (y), and spanwise (z) directions, respectively.

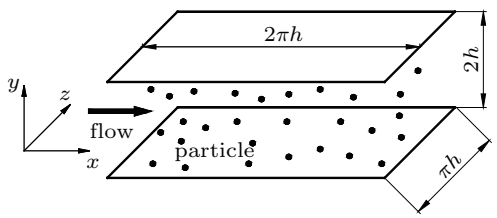


Fig. 1. Schematic diagram of particle-laden turbulent airflow in a channel.

LES is employed to simulate the turbulent airflow. The three-dimensional incompressible continuity and Navier–Stokes equations are shown in Eqs. (1) and (2), respectively, after using a classical box filter:

$$\frac{\partial \bar{u}_i}{\partial x_i} = 0, \tag{1}$$

$$\frac{\partial \bar{u}_i}{\partial t} + \frac{\partial}{\partial x_j}(\bar{u}_i \bar{u}_j) = -\frac{\partial p}{\partial x_i} + \frac{1}{Re_\tau}\frac{\partial^2 \bar{u}_i}{\partial x_j \partial x_j} - \frac{\partial \tau_{ij}}{\partial x_j}, \tag{2}$$

where $\bar{u}_i$ and $\bar{u}_j$ are the velocity components, and P is pressure. The friction Reynolds number based on the friction velocity u_τ and half channel height H is $Re_\tau = u_\tau H/\eta$. η is the fluid kinematic viscosity, and τ_{ij} is the sub-grid-scale stress, which is approximated by the eddy viscosity hypothesis as

$$\tau_{ij} = -2\mu_T \bar{S}_{ij} + \frac{1}{3}\delta_{ij}\tau_{kk}. \tag{3}$$

The eddy viscosity μ_T and strain rate tensor $\bar{S}_{ij}$ are defined as

$$\mu_T = \rho C_{SGS} \Delta_s^2 \left|\bar{S}\right|, \tag{4}$$

$$\bar{S}_{ij} = \frac{1}{2}\left(\frac{\partial \bar{u}_i}{\partial x_j} + \frac{\partial \bar{u}_j}{\partial x_i}\right), \tag{5}$$

where C_{SGS} is an empirical constant (taken to be 0.1 in this study). For the channel flow, a damping function f_s is applied to Eq. (4), because the Smagorinsky model has overlarge dissipation predictions near the wall and the viscosity must be zero at the wall. A Van Driest-type damping function $f_s = 1 - \exp(-y^+/25)$ is employed in the simulation, where y^+ is the distance from the wall.

Equations (1) and (2) are solved using a fractional step method.[28] The viscous term is discretized by a second-order central scheme and the advective term is discretized using a second-order hybrid scheme to reduce aliasing errors and instability. The momentum equations are integrated explicitly using the third-order Runge–Kutta algorithm. The pressure Poisson equation is solved by means of Fourier series expansions in the streamwise and spanwise directions with tridiagonal matrix inversion. Periodic boundary conditions are applied in the streamwise and spanwise directions. No-slip boundary conditions are imposed at the walls for fluids.

A constant mean pressure-gradient in the streamwise direction drives the flow, and the flow friction Reynolds number is set to 180. Staggered grids are used in the simulations, with 262,144 grid points in the x, y, and z directions. The grids are uniform in the streamwise and spanwise directions, whereas the grid points are denser in the near-wall region in the direction normal to the wall according to the hyperbolic tangent function

$$y = \frac{\tanh(a(\xi - 0.5))}{\tanh(a/2)}. \tag{6}$$

In wall units, the grid spacings are $\Delta x^+ = 17.93$, $\Delta z^+ = 8.82$, $\Delta y^+_{min} = 0.49$ near the wall and $\Delta y^+_{max} = 11.42$ at the center of the channel. The Kolmogorov scale of turbulent flow at the present Reynolds number is about two wall units.[29] As the present gird space never exceeds ten times the Kolmogorov scale, the sub-grid scale turbulence effects on particle motion can be ignored.

2.2. Lagrangian trajectory method for the particle phase

To describe the particle motion, a Lagrangian trajectory method is employed under the assumption of one-way coupling. The modification of particles in turbulent airflow and the interaction between particles are ignored, because the particle concentration in this study is very dilute. The particles are assumed to be spheres. The particle diameter is sufficiently small compared with the Kolmogorov length scale that the point force model can be used to simulate the particle motion. Under such conditions, the particles are governed only by the Stokes drag force,[30] as other particle forces are significantly smaller. The particle equation of motion is

$$\frac{\mathrm{d}\upsilon_i}{\mathrm{d}t} = -\frac{\rho_\mathrm{f}}{\rho_\mathrm{p}}\frac{3}{4}\frac{C_\mathrm{D}}{d_\mathrm{p}}|\boldsymbol{v}-\boldsymbol{u}|(\upsilon_i - u_i), \tag{7}$$

where υ_i and u_i are the particle and the fluid velocities at the particle position, respectively; ρ_f and ρ_p are the fluid and particle densities, respectively; and d_p is the particle diameter. C_D is the drag coefficient, which is given by

$$C_\mathrm{D} = \frac{24Cr}{Re_\mathrm{p}}, \tag{8}$$

where Re_p is the particle Reynolds number, $Re_\mathrm{p} = d_\mathrm{p}|\boldsymbol{v}-\boldsymbol{u}|/\eta$, η is the fluid kinematic viscosity, and $Cr = (1 + 0.15Re_\mathrm{p}^{0.678})$ is the correction coefficient. The fluid velocities seen by the particles are obtained by interpolating the fluid velocities of the staggered meshes to the particle locations using a fourth-order Lagrangian interpolation. If the particle is located at $(x_\mathrm{p}, y_\mathrm{p}, z_\mathrm{p})$ and its nearby coordinates are $(x_0, y_0, z_0), \ldots, (x_l, y_l, z_l)$, the Lagrangian interpolation can be given as

$$u_{\mathrm{f@p}}(x_\mathrm{p}, y_\mathrm{p}, z_\mathrm{p}) = \sum_{i=1-n/2}^{n/2}\sum_{j=1-n/2}^{n/2}\sum_{k=1-n/2}^{n/2}\left(\prod_{\substack{l=1-n/2\\(l\neq i)}}^{n/2}\frac{x_\mathrm{p}-x_l}{x_i-x_l} \times \prod_{\substack{l=1-n/2\\(l\neq j)}}^{n/2}\frac{y_\mathrm{p}-y_l}{y_j-y_l}\prod_{\substack{l=1-n/2\\(l\neq k)}}^{n/2}\frac{z_\mathrm{p}-z_l}{z_k-z_l}\right)\boldsymbol{u}_{i,j,k}, \tag{9}$$

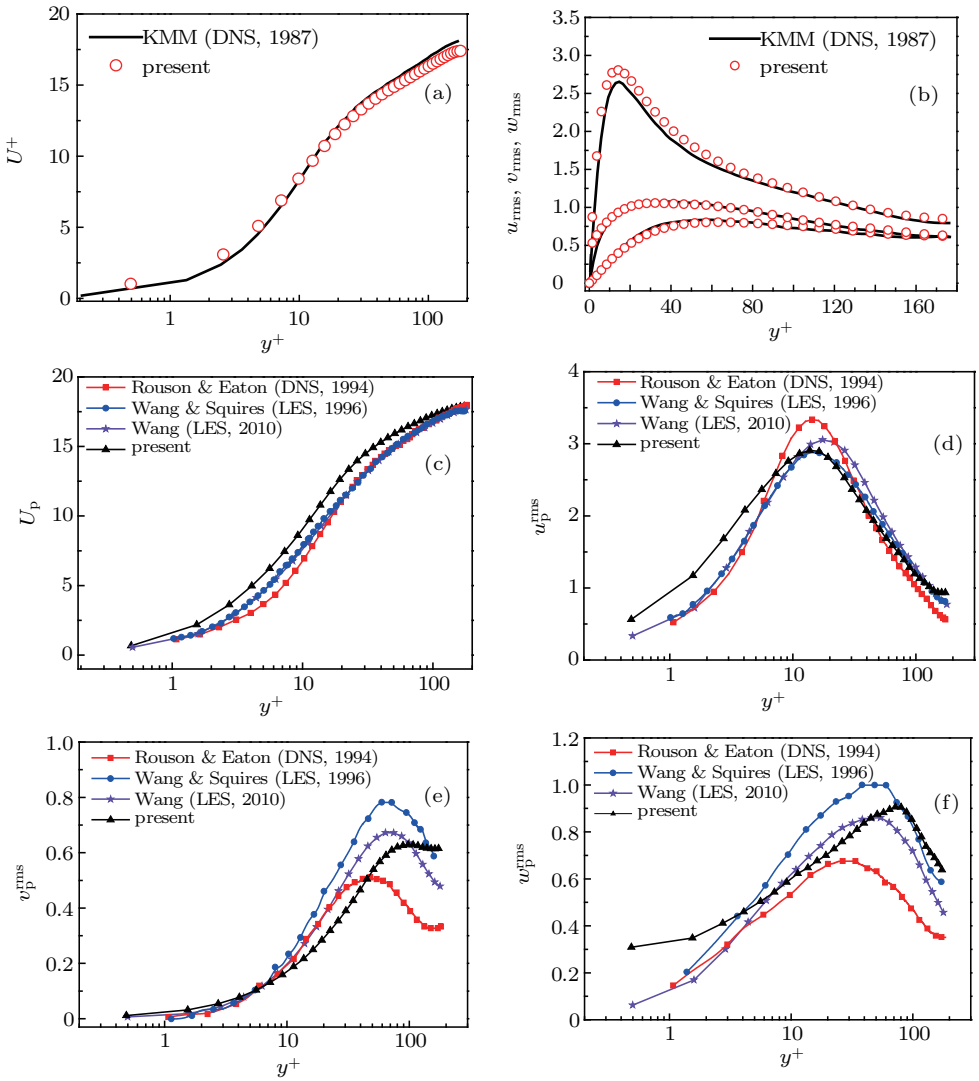


Fig. 2. (color online) Mean velocities for fluid phase (a) and particle phase (c), and fluctuating velocity for fluid phase (b) and particle phase: streamwise fluctuating velocity (d), wall-normal fluctuating velocity (e), and spanwise fluctuating velocity (f).

where i, j, k, and l are the cell indexes and $n = 4$. The particle density is 700 kg/m^3 and the particle diameter is 30 μm. The Stokes number is approximately 1. The Stokes number ($St = \tau_{rp}/\tau_f$) is based on the Kolmogorov timescale of turbulent flow. τ_{rp} and τ_f are the particle relaxation time and characteristic fluid timescale, respectively. τ_{rp} can be calculated by

$$\tau_{rp} = \frac{\rho_p d_p^2}{18\mu}, \tag{10}$$

where ρ_p and d_p are the density and diameter of the particles, respectively, and μ is the dynamic coefficient of viscosity. τ_f can be computed as

$$\tau_f = h/U_c, \tag{11}$$

where h is half the channel height and U_c is the center velocity of the air channel flow. The friction Reynolds number is 180. The corresponding flow Reynolds number is 3300, based on the mean centerline velocity and channel half-height. The number of particles released into the flow fields is 150,000. The corresponding particle mass loading ratio is 0.08%. A periodic boundary condition is adopted at the inlet and outlet of the channel. This means that particles moving out of the computational domain from the outlet pass into the channel again from the inlet. Perfectly elastic collisions at the walls are assumed when the particle center is at a distance less than one particle radius from the wall.

2.3. Numerical simulation verification

To verify the present numerical methods and the in-house codes, the mean and fluctuating velocities of fluids and particles were calculated and compared with previous data in the related literature (see Fig. 2). The mean velocities and fluctuating velocities are all normalized according to the frictional velocity u_τ. It can be observed that the mean and fluctuating velocities of fluids from the present LES agree very well with the DNS results of Kim *et al.*,[29] as shown in Figs. 2(a) and 2(b). This indicates that the turbulent airflow is well resolved by the present numerical methods and codes. Moreover, the statistical mean and fluctuating velocity profiles of particles are also compared with previous DNS and LES data reported by Wang and Squires[26] and Wang,[31,32] as shown in Figs. 2(c)–2(f). It can be observed that both the mean and fluctuating velocities of particles are in good agreement with the previous results. These verifications indicate that the present numerical algorithms simulate the particle motion very well.

3. Preferential concentration of particles

The preferential concentration refers to the tendency of dense particles in a turbulent flow to present inhomogeneous spatial distributions, forming clusters and depleted regions. In this study, we focus on particle dispersion and transport mechanisms in the well-developed turbulent airflow. The preferential concentration of particles in turbulent airflow is illustrated in Fig. 3. Three-dimensional spatial distributions of particles overlaid with the iso-surface of the Q-criterion are displayed in Fig. 3(a). The colors in Fig. 3(a) represent the streamwise fluctuation of airflow velocities. To investigate the relevance of turbulent vortex structures and particle spatial distributions, the Q-criterion, which was developed by Hunt *et al.*,[33] is used to display intense vortical structures in turbulent airflow. The Q-criterion represents the normalized second invariant of the velocity gradient tensor, and is defined as

$$Q = \frac{1}{2}(\Omega_{ij}\Omega_{ij} - S_{ij}S_{ij}), \tag{12}$$

where $\Omega_{ij} = 0.5(\partial u_i/\partial x_j - \partial u_j/\partial x_i)$ and $S_{ij} = 0.5(\partial u_i/\partial x_j + \partial u_j/\partial x_i)$ are the symmetric and anti-symmetric parts of the velocity gradient tensor, respectively. Positive values of the Q-criterion indicate regions where flow rotation dominates over straining. Large-scale turbulent vortical structures within the 150,000 particles can be observed in Fig. 3(a). The particles present a three-dimensional highly non-uniform structure in the airflow fields, and obviously cluster in the regions of low vorticity.

Figure 3(b) shows the spatial distributions of particles with $St = 1$ overlaid with instantaneous streamwise velocity fields of fluids in the vertical XY plane at $Z = 1.57$. It is clear that the particles form obvious clusters and depleted regions in the flow fields, and become preferentially concentrated in the near-wall regions, as shown by the arrows in the figure. Figure 3(c) shows the spatial distributions of particles overlaid with instantaneous streamwise fluctuating velocities of fluids in the near-wall XZ plane at $y^+ = 5.6$. The streaked patterns in Fig. 3(c) are low-speed regions in the streamwise direction, which produce low-speed streaky structures in the near-wall region. Low-speed streaks are typical large-scale turbulent coherent structures induced by quasi-streamwise vortices (QSVs). The generation of low-speed streaks is spatiotemporally indeterminate, although once generated they rise, oscillate, and finally break up with strong ejections. It is observed that particles obviously cluster in low-speed streaks very near the wall at $y^+ = 5.6$, as shown in Fig. 3(c). Moreover, the patterns of particle streaks are very similar to the fluid phase. This indicates the strong preferential concentration of particles in the near-wall region, approximately in the viscous sublayer. The above results indicate that intense particle clusters appear in the near-wall and low-speed regions of the turbulent flow.

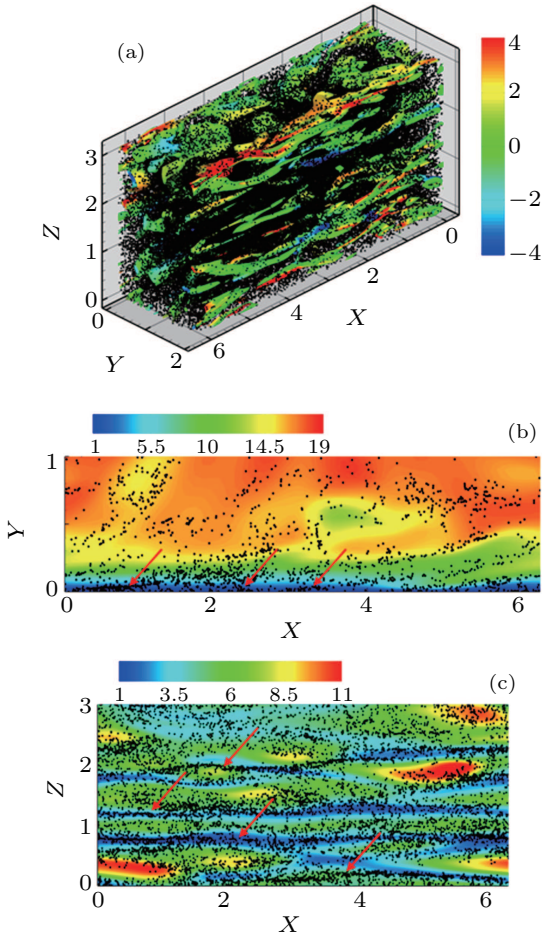


Fig. 3. (color online) Non-uniform spatial distribution of particle with St=1 in turbulent airflow fields. (a) Three-dimensional spatial distributions of particles and iso-surface of the Q-criterion. Spatial distributions of particles in the vertical plane of $Z = 1.57$ (b) and in the near-wall plane at $y^+ = 5.6$ (c).

The particle number density profile versus the distance to the wall is shown in Fig. 4. It can be seen that the maximum particle number density appears in the viscous sublayer ($y^+ < 5$), and can reach 3.2%. The particle number density then decreases rapidly as the distance to the wall increases ($5 < y^+ < 40$). In the middle and center layers ($y^+ > 40$), the particle number density remains almost constant at approximately 0.5%.

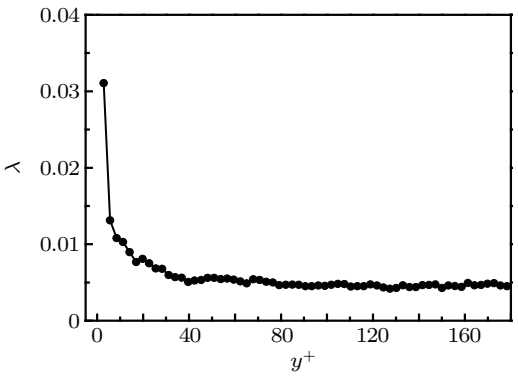


Fig. 4. The particle number density profile versus the distance to the wall.

4. Spatiotemporal evolution of particles transport in airflow fields

4.1. Multi-group Lagrangian tracking

The particle behavior in different flow field regions of turbulent channel flow is strongly affected by the turbulent structures and flow characteristics. However, the traditional Lagrangian tracking method cannot identify these differences, because all of the particles are tracked together. Thus, it is difficult to distinguish where the particles have been and where they are going. To resolve this problem, a multi-group Lagrangian tracking method is proposed in this study. As the low-speed streaks and near-wall structures are significant regions in turbulent channel flow, the flow regions are divided into three regions in the wall-normal direction, as shown in Fig. 5(a): the first region is $0 < y^+ < 40$, where low-speed streaks exist;[34] the second region is $40 < y^+ < 100$, as the near-wall region is defined as $y^+ < 100$;[34] and the third region is $100 < y^+ < 180$, as the center of the channel flow is at $y^+ = 180$. These three regions are defined as streaky layer, middle layer, and center layer, respectively. The streaky layer is divided into a low-speed streaky region and the region with no low-speed streaks, as shown in Fig. 5(b). Particles in the different flow regions have different dispersion characteristics. Therefore, the particles are divided accordingly into the four groups shown in Figs. 5(a) and 5(b): particles in the low-speed streaks ($y^+ < 40$), particles outside the low-speed streaks ($y^+ < 40$), particles in the middle layer ($40 < y^+ < 100$), and particles in the center layer ($100 < y^+ < 180$). These are referred to as inner particles, outer particles, middle particles, and center particles, respectively. The trajectories of the four groups of particles are recorded once the fluid is fully developed.

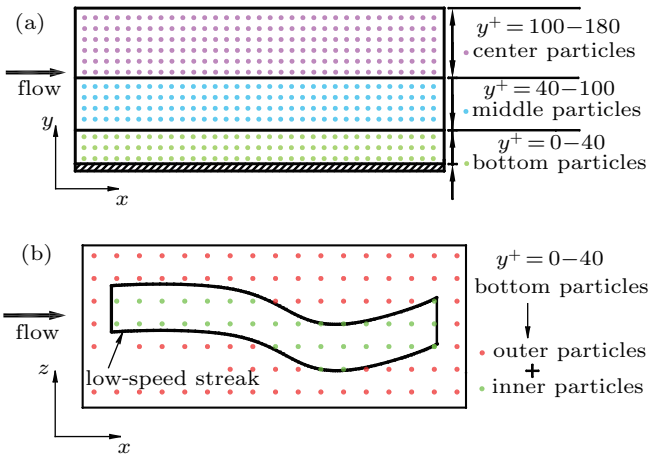


Fig. 5. (color online) Partitions of flow fields and particles: divided in y direction (a) and in z direction (b).

4.2. Spatiotemporal evolution of multi-groups of particles

Once the turbulent gas–particle flow is fully developed at $t = 150$, the particles in low-speed streaks at this time are marked and named inner particles. The spatial distribution of these inner particles is then tracked over the period $t = 150$–155.25, as shown in Fig. 6. It is observed that all particles are in low-speed streaks at $t = 150$, as shown in Fig. 6(a), and no particles are in the middle layer or the center layer shown in Figs. 6(b) and 6(c). When $t = 150.25$, most particles are still in low-speed streaks, although some have been transported into the middle layer, as shown in Figs. 6(d) and 6(e). Note that the inner particles in the middle layer shown in Fig. 6(e) are distributed similarly to those in the low-speed streaks in Fig. 6(d). It can be concluded that these inner particles are directly entrained up to the middle layer by the ejection of wall turbulence. At $t = 151.25$, more inner particles have been transported into the middle layer, and these particles begin to diffuse in the spanwise direction under spanwise fluctuations in turbulence, as shown in Fig. 6(h). However, there are still particle streaks in the middle layer at this time. Moreover, some inner particles in the middle layer have been transported into the center layer, as shown in Fig. 6(i). This indicates that the inner particles are not just clustered in low-speed streaks all the time, but are transported and dispersed in the whole channel flow. When $t = 152.25$ and 155.25, there are still a large number of particles clustered in low-speed streaks; however, the patterns and positions of the low-speed streaks have varied. This indicates that most of the particles will reside in low-speed streaks for a long period once they have been captured.

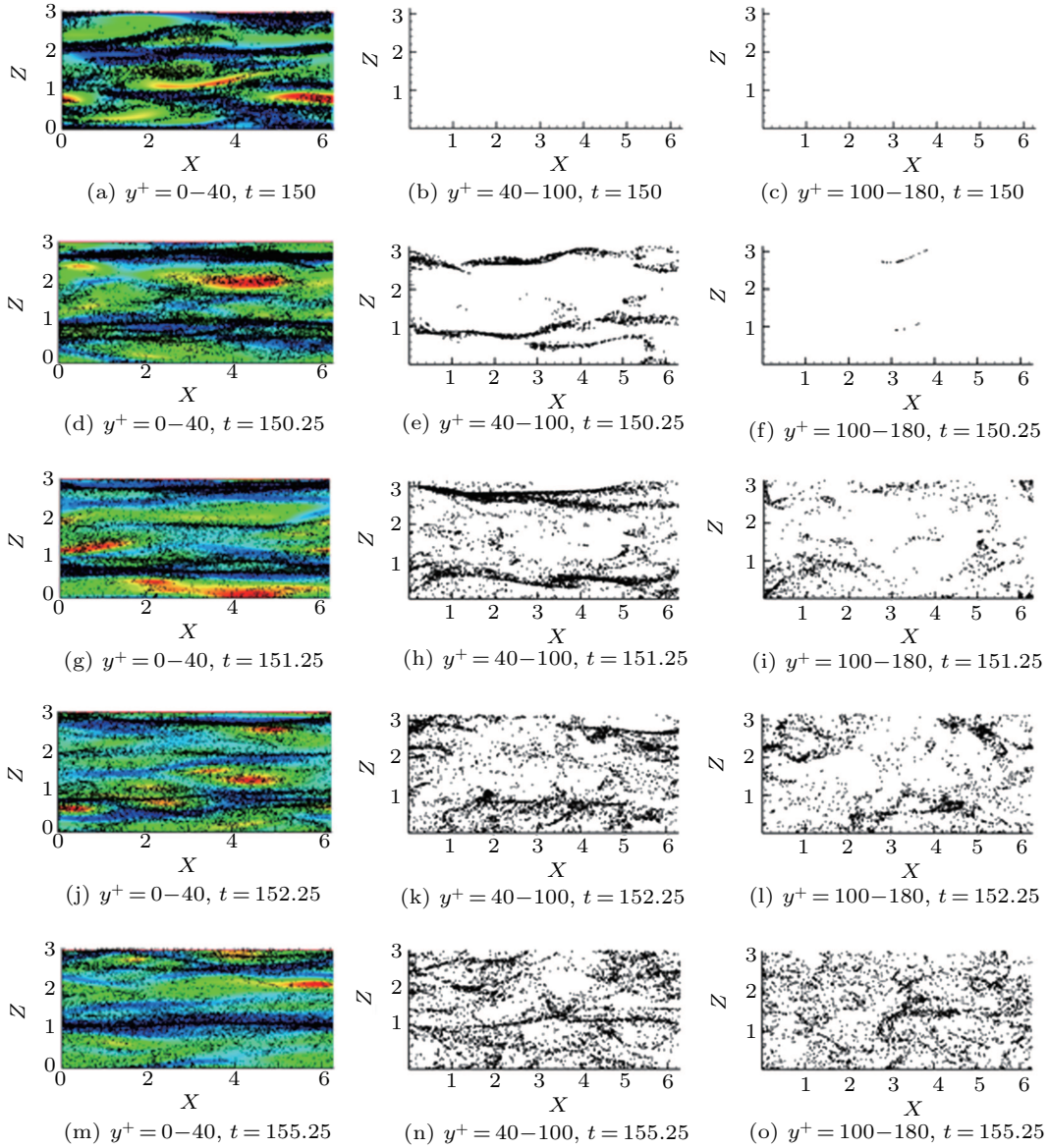


Fig. 6. (color online) Temporal evolutions of spatial distributions of the inner particles.

The spatial distribution of the outer particles was also investigated over the period $t = 150$–155.25, as shown in Fig. 7. It can be observed that all the particles are outside of the low-speed streaks at $t = 150$, and no particles appear in the middle layer or the center layer, as shown in Figs. 7(a)–7(c). When $t = 150.25$, some of the outer particles have become clustered in the low-speed streaks, and a few have been transported into the middle layer, as shown in Figs. 7(d) and 7(e). These outer particles in the middle layer appear as similar particle streaks with turbulence. These results demonstrate that a portion of the outer particles are first transported into the low-speed streaks through spanwise migration, and are then entrained by ejections of turbulence into the middle layer. Therefore, entrainment by ejection is the main mechanism of particle transport to the middle layer from the streak layer, whether for inner particles or outer particles. When the outer particles move into low-speed streaks, their dispersion is very similar to that of the inner particles discussed above. Some of the outer particles move into the middle and center layers. It is interesting that the distributions of outer particles in the three layers are very similar to those of the inner particles at $t = 155.25$.

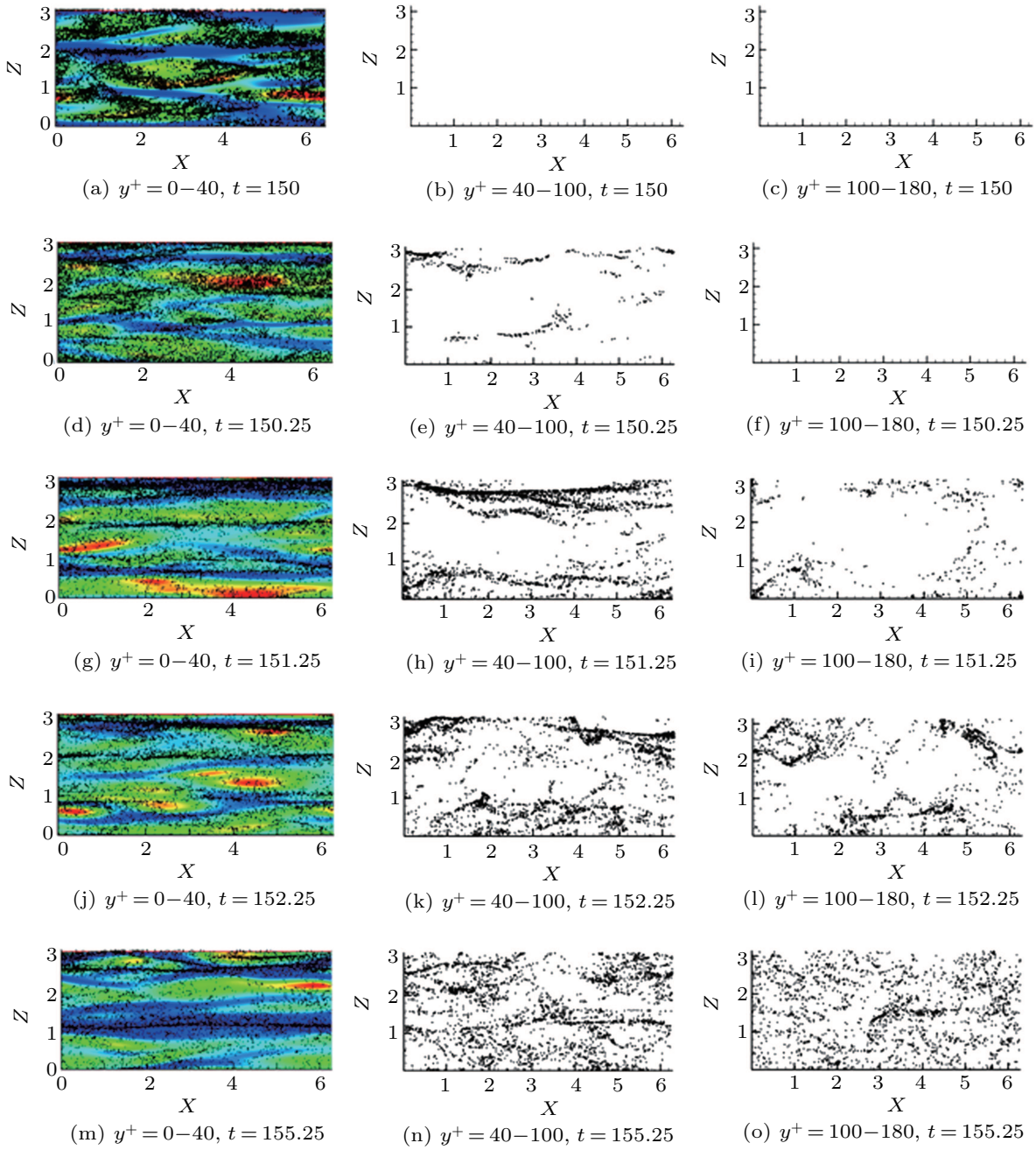


Fig. 7. (color online) Temporal evolutions of spatial distributions of the outer particles.

Figure 8 shows the temporal evolution of the spatial distribution of the middle particles. These particles are only in the middle layer when $t = 150$, as shown in Fig. 8(b). Some of the middle particles are then conveyed into the streak and center layers at $t = 150.25$, as shown in Figs. 8(d) and 8(f). Note that the particles in the streak layer are strongly preferentially concentrated in the regions of high streamwise velocity, as shown by Fig. 8(d). When $t = 151.25$, the particles in the streak layer begin to diffuse into the low-speed streaks, as shown in Fig. 8(g). Thus, the outer particles are captured by sweeps of turbulence and transported to high-speed regions of the streak layer first, and are then diffused into the low-speed streaks. An increasing number of middle particles move into the streak layer and accumulate in low-speed streaks with time, as shown in Figs. 8(j) and 8(m). At the same time, some of the middle particles are also transported to the center layer, forming particle clusters.

Finally, the temporal evolution of the spatial distribution of the center particles is presented in Fig. 9. The center particles are only in the center layer when $t = 150$, as shown in Fig. 9(c). Some of the center particles have been conveyed into the middle layers by $t = 150.25$, as shown in Fig. 9(e). The transport process of the center particles is then similar to that of the middle particles. Finally, a number of center particles also cluster in low-speed streaks in the streak layer, as shown in Fig. 9(m).

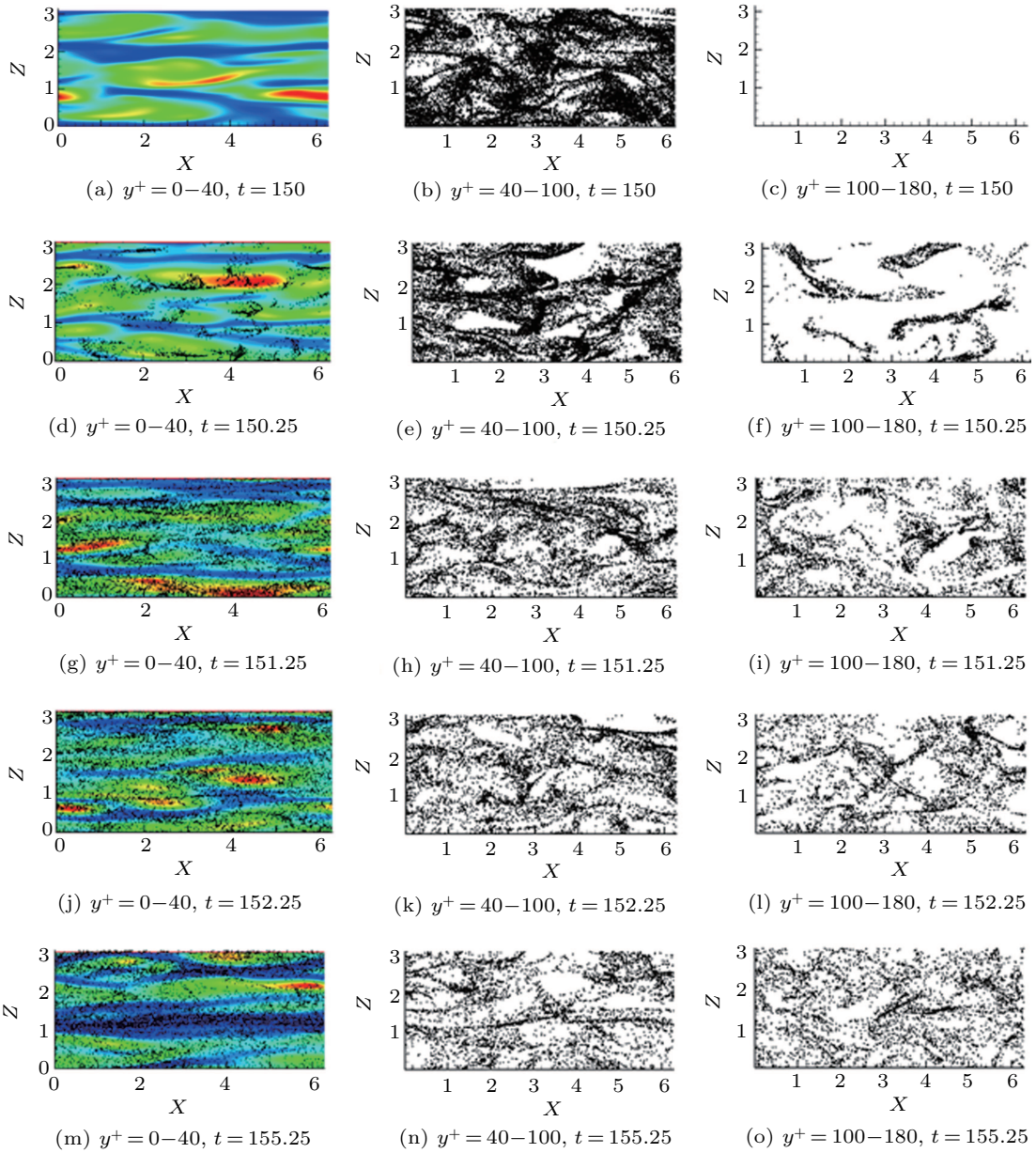


Fig. 8. (color online) Temporal evolutions of spatial distributions of the middle particles.

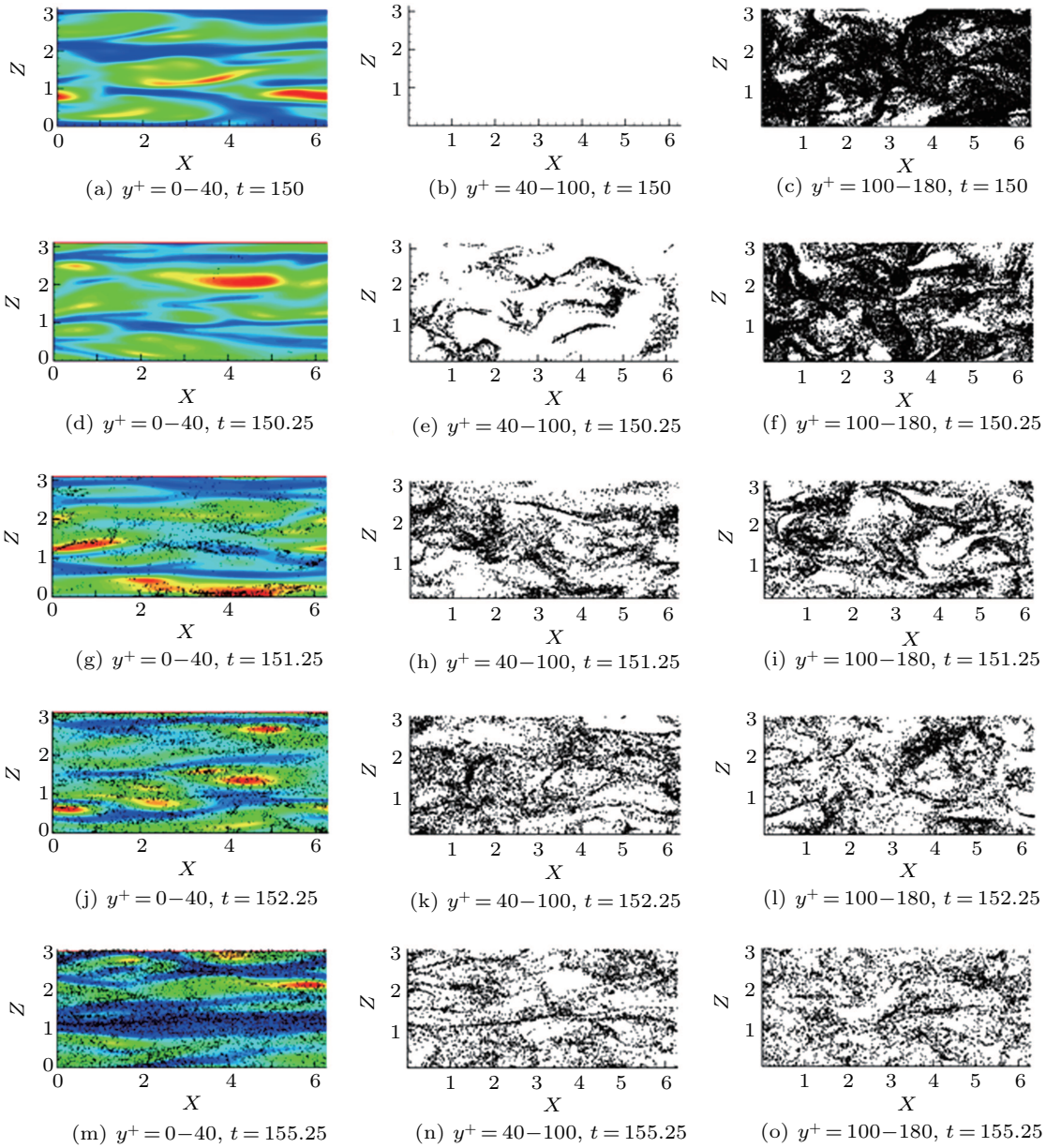


Fig. 9. (color online) Temporal evolutions of spatial distributions of the center particles.

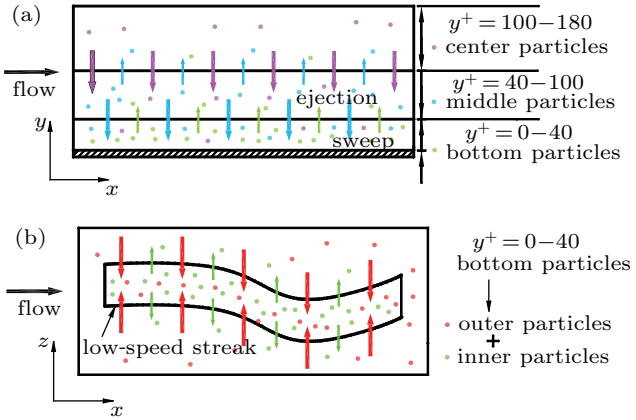


Fig. 10. (color online) Particle migration routes in turbulent boundary layer. Particle migrations in the wall-normal direction (a) and in the spanwise direction (b).

Based on the above analysis, a schematic diagram of the particle migrations in turbulent airflow is summarized in Fig. 10. Ejections and sweeps of turbulence are the main mechanisms for transporting particles toward or away from the wall in the turbulent boundary layer. In the near-wall regions, particles are transported to low-speed streaks through spanwise migration.

4.3. Mechanisms of particle transport

The number of particles entering or leaving the low-speed streaks is shown in Fig. 11. It can be observed that 40–100 particles entered the low-speed streaks, whereas 25–80 moved away from the low-speed streaks. As the particle flux into the low-speed streaks is greater than that moving out of the low-speed streaks, particle clusters can be observed in this region.

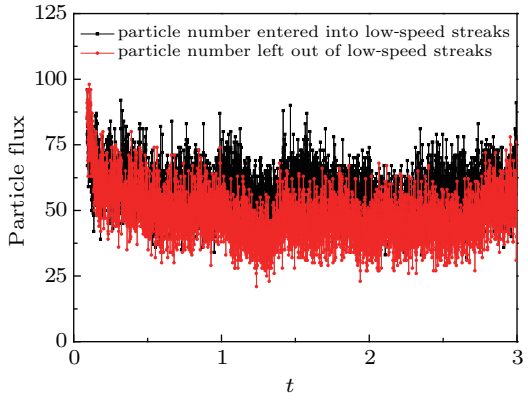


Fig. 11. (color online) Particle flux entered into and left out of low-speed streaks.

Moreover, the transverse exchange of particles between the inner and outer regions is mainly influenced by the spanwise particle velocity fluctuations. To investigate the mechanism of particle transverse exchange in low-speed streaky structures, figure 12 shows the statistical spanwise velocity fluctuations of inner particles, outer particles, and all of the particles in the streaky layer. The statistics are obtained from $y^+ = 0$–40 in the wall-normal direction, because turbulent streaky structures exist in this region.[34] It can be seen that the spanwise velocity fluctuations of inner particles are significantly weaker than those of outer particles. This implies that the inner particles find it difficult to escape from the low-speed streaks once they have been captured. On the contrary, the outer particles are more likely to be transported into the low-speed streaks because they are active and unstable in regions of high streamwise velocity. Therefore, the particle flux into the low-speed streaks is positive. This mechanism results in a large number of particles clustered in low-speed streak structures.

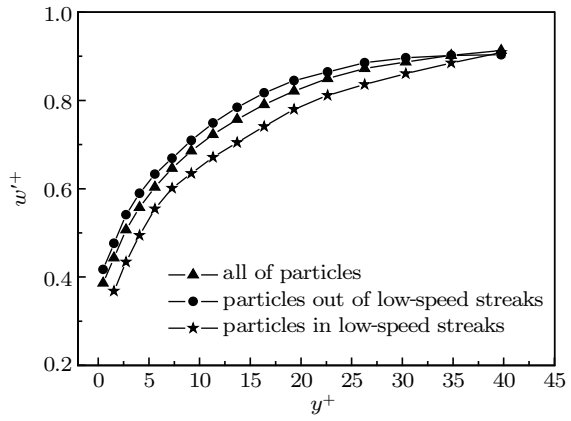


Fig. 12. Spanwise fluctuating velocities of particles in the streaky layer.

To investigate the particle trajectory following the vortex evolution, figure 13 shows the particle spatial distribution overlaid on the vorticities in the YZ plane at $X = 3.14$. The arrows and colors in the figure represent the velocity vectors in the plane and the vorticity values. The large-scale QSVs can be clearly observed. Moreover, it can be seen that the middle particles were captured by QSV and entrained into the streaky layer through the sweep motions, as shown by the arrows in Fig. 13. These particles were transported in the spanwise direction by the vortex motion. The breakup of a QSV can be observed. This induces intense ejection motion. A large number of particles are transported into the middle layer by this vortex breakup, as shown by the arrows. Therefore, the near-wall QSV evolution, including sweep and ejection motions, is the main mechanism of particle transport in the near-wall regions.

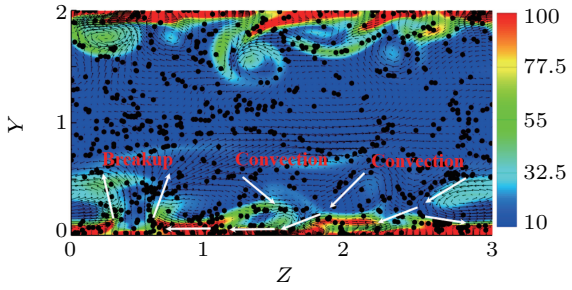


Fig. 13. (color online) Particle trajectory following the vortex evolution in YZ plane at $X = 3.14$.

5. Conclusion

The detailed particle transport processes and mechanisms in turbulent airflow have been investigated by means of LES and the Lagrangian trajectory method. The detailed evolution processes of particle transport and clustering in the near-wall region and low-speed streaks were studied by tracking four groups of particles. The results showed that although some of the inner particles are transported to the middle layer through the entrainment of ejections, most particles still accumulate in low-speed streaks for a long period. Outer particles immediately move to low-speed streaks, where they are subjected to similar transport processes as the inner particles. Most of the middle particles are captured by the sweeps and conveyed into the high streamwise velocity regions of the streak layer. They also diffuse in low-speed streaks through the spanwise movements. Center particles are transported to the middle layer, and then become middle particles with similar dispersion behavior. Over time, the four groups of particles all preferentially concentrate in the low-speed streaks of the near-wall regions.

References

[1] Shao X M, Lin J Z, Wu T and Wu Y L 2002 *Can. J. Chem. Eng.* **80** 293
[2] Chan T L, Lin J Z, Zhou K and Chan C K 2006 *J. Aerosol Sci.* **37** 1545
[3] Jin G D, He G W, Wang L P and Zhang J 2010 *Int. J. Multiphase Flow* **36** 432
[4] Lu H, Wang B, Zhang H Q and Wang X L 2013 *Sci. China-Phys. Mech.* **56** 645
[5] Lu H, Wang B, Zhang H Q, Qin J X and Wang X L 2013 *Sci. China-Technol. Sci.* **56** 2525
[6] Crowe C T, Chung J N and Troutt T R 1988 *Prog. Energy Combust. Sci.* **14** 171

[7] Crowe C T, Gore R A and Troutt T R 1985 *Partic. Sci. Technol. J.* **3** 149
[8] Squires K D and Eaton J K 1990 *Phys. Fluids A* **2** 1191
[9] Squires K D and Eaton J K 1991 *Phys. Fluids A* **3** 1169
[10] Wang L P and Maxey M R 1993 *J. Fluid Mech.* **256** 27
[11] Wang L P and Maxey M R 1993 *Appl. Sci. Res.* **51** 291
[12] Longmire E K and Eaton J K 1992 *J. Fluid Mech.* **236** 217
[13] Crowe C T, Sommerfeld M and Tsuji T 1998 *Multiphase Flows with Droplets and Particles* (New York: CRC Press)
[14] Crowe C T 2006 *Multiphase Flow Handbook* (New York: CRC Press)
[15] Balachandar S and Eaton J K 2010 *Annu. Rev. Fluid Mech.* **42** 111
[16] Luo K, Fan J R, Li W C and Cen K F 2009 *Fuel* **88** 1294
[17] Luo K, Gui N, Fan J R and Cen K F 2013 *Int. J. Heat Mass Tran.* **64** 155
[18] Luo K, Fan J R, Jin H H and Cen K F 2004 *Powder Technol.* **147** 49
[19] McLaughlin J B 1989 *Phys. Fluids A* **1** 1211
[20] Brooke J W, Kontomaris K, Hanratty T J and McLaughlin J B 1992 *Phys. Fluids A* **4** 825
[21] Eaton J K and Fessler J R 1994 *Int. J. Multiphase Flow* **20** 169
[22] Kaftori D, Hetsroni G and Banerjee S 1995 *Phys. Fluids* **7** 1095
[23] Kaftori D, Hetsroni G and Banerjee S 1995 *Phys. Fluids* **7** 1107
[24] Tanaka M, Maeda Y and Hagiwara Y 2002 *Int. J. Heat Fluid Fl.* **23** 615
[25] Fessler J R, Kulick J D and Eaton J K 1994 *Phys. Fluids A* **6** 3742
[26] Wang Q and Squires K D 1996 *Phys. Fluids* **8** 1207
[27] Monchaux R, Bourgoin M and Cartellier A 2012 *Int. J. Multiphase Flow* **40** 1
[28] Chorin A J 1968 *Math. Comp.* **22** 745
[29] Kim J, Moin P and Moser R 1987 *J. Fluid Mech.* **177** 133
[30] Maxey M and Riley J 1983 *Phys. Fluids* **26** 883
[31] Wang B 2010 *Int. J. Heat Mass Tran.* **53** 2506
[32] Wang B 2010 *Int. J. Heat Mass Tran.* **53** 2522
[33] Hunt J C, Wray A A and Moin P 1988 *Tech. Rep.* CTR-S88
[34] Pope S 2000 *Turbulent Flows* (Cambridge: Cambridge University Press)